Nanoscale

Cite this: *Nanoscale*, 2012, **4**, 1476

www.rsc.org/nanoscale

COMMUNICATION

High-yield synthesis of ZnO nanowire arrays and their opto-electrical properties†

Chen-Yen Kao,[a] Cheng-Lun Hsin,[a] Chun-Wei Huang,[a] Shih-Ying Yu,[a] Chun-Wen Wang,[a] Ping-Hung Yeh[b] and Wen-Wei Wu*[a]

Received 6th July 2011, Accepted 21st September 2011
DOI: 10.1039/c1nr10742a

In this article, ZnO nanostructures were synthesized *via* the hydrothermal method which used $ZnCl_2$ and HMTA mixed solution as the precursor. A multistep growth was adopted to improve the growth restriction of a closed system, not only the length but also the aspect ratio were increased with steps of growth, and the shape of nanorods maintained integrity. Furthermore, photoluminescence spectra which have the near-band-edge-emission (~3.37 eV) and defect-related emission show the optical properties of ZnO nanostructures. The defect-related emission intensity was greatly enhanced with the increasing surface area of ZnO nanowires. The level of the OH group was attributed to the yellow-light emission (~580 nm) and the red-shift phenomenon. In addition, we fabricated two types of ultraviolet photodetectors: a single nanowire device and a nanowire-array device, operating at a low bias (less than 5 mV). With the lower energy consumption and the weaker persistent photoconductive effect, our ultraviolet photodetectors have better performance, exhibiting a short response time and higher sensitivity.

Introduction

ZnO is an important II–VI compound semiconductor material, with a wide direct band gap (3.37 eV) and high exciton binding energy. It has been demonstrated that ZnO has various applications in electronics, optoelectronics, electromechanical, and electrochemical nanodevices, including ultraviolet (UV) lasers,[1] light-emitting diodes,[2] field-emission devices,[3] solar cells,[4,5] high performance nanosensors,[6–8] and piezoelectric nanogenerators.[9] The performance of the devices is related to the electrical, thermal transport, optical, and mechanical properties of ZnO. Various types of nanostructures, such as nanowires (NWs), nanotubes (NTs), nanobelts (NBs), and nanorods (NRs), have been synthesized and extensively studied. To date, different methods have been developed to synthesize ZnO nanostructures, including a sol–gel process, hydrothermal method,[10–14] electrochemical reaction,[15] thermal evaporation,[16,17] and laser ablation.[18] Among these methods, the hydrothermal method has the advantages of low temperature, large scale productivity, and economical synthesis. In general, the growth solution of the hydrothermal method contains zinc salt and organic amine such as hexamethylenetetramine (HMTA, $(CH_2)_6N_4$).[10,19] Furthermore, a seed layer of ZnO thin film is required to improve the alignment of ZnO nanostructures.

For ZnO nanostructured photodetectors, the generation of a photocurrent is attributed to the incident radiation, resulting in the electrical conductivity change. There are two primary mechanisms to control the photoresponse. The first one is the band-to-band recombination in the bulk material and the response time is in the nanosecond range. The other is the hole-trapping mechanism based on the adsorbed oxygen molecules at the surface.[20] The electron–hole pairs are photogenerated by UV illumination and the photogenerated holes would migrate to neutralize oxygen at the surface. Then, the electrons of electron–hole pairs remain and therefore contribute to the photoconductivity. The above theory indicates that the photoresponsivity of ZnO NWs can be enhanced by increasing the amount of adsorbed oxygen at the surface.

In this paper, high-yield ZnO NWs with a [0001] growth direction have been synthesized by a hydrothermal method. The multistep growth was adopted to improve the aspect ratio. Photoluminescence (PL) results revealed that the optical properties are related to the surface area and OH group. Photodetectors of a ZnO single NW and ZnO aligned NW arrays were applied with a low bias (less than 5 mV) and the mechanism of the photoresponse of the photodetectors was investigated. The less slowly decayed photocurrent and enhanced photoswitching speed were observed in the devices with a low bias. These results demonstrated that applying a lower external electrical field can improve the photoresponsivity of both single NW and aligned NW array devices.

Experimental methods

The ZnO NWs were synthesized on a Si (100) substrate using the hydrothermal method. A 100 nm thick seed layer was deposited on the Si substrate by RF sputtering. The growth precursors consisted of

[a]*Department of Materials Science and Engineering, National Chiao Tung University, No. 1001, University Rd, East Dist., Hsinchu City, 300, Taiwan. E-mail: wwwu@mail.nctu.edu.tw; Fax: +886-3-5724727; Tel: +886-3-5712121-55395*

[b]*Department of Physics, Tamkang University, No. 151 Yingzhuan Rd, Danshui Dist., New Taipei City, 25137, Taiwan; Fax: +886-2-2620-9917; Tel: +886-2-26215656-2819*

† This article was submitted as part of a collection highlighting papers on the 'Recent Advances in Semiconductor Nanowires Research' from ICMAT 2011.

a 5 mM solution of $ZnCl_2$ and HMTA in DI water which were prepared and then the face-downward substrate was suspended in solution. Then, the solution was maintained at 90 °C for 12 h. After growth, the substrate was removed from the solution and then dried in the oven. In addition, the aligned ZnO NW array photodetectors were made of the as-grown samples with parallel colloidal silver pads as the electrodes. Au (120 nm)/Ti (30 nm) were deposited as contact metals of the electrodes of the ZnO single NW photodetectors by the techniques of photolithography, e-beam lithography, and e-gun deposition.

The ZnO NWs were characterized by the X-ray diffractometer (XRD, Bruker D2 phaser) using the Cu K_α radiation ($\lambda = 1.5406$ nm) and a high resolution transmission electron microscope (HRTEM, JEOL JSM-2100F). The morphology was examined by a field-emission scanning electron microscope (FESEM, JEOL JSM-6500F). A room temperature PL with a 325 nm He–Cd laser was used to study the optical properties of the ZnO NWs. The electrical properties and photoresponsivity were measured by semiconductor analyzers (Agilent B1500A and Keithley 2400). Furthermore, the photoresponse properties of ZnO photodetectors were examined with a 4 W UV lamp and the intensity is 8 mW cm^{-2}.

Results and discussion

Structure analysis

The as-grown samples were examined by FESEM. Fig. 1(a) shows the SEM image of ZnO NW arrays with uniform diameter in the range of 60–120 nm and the length up to several microns. The XRD data taken from the ZnO NW arrays on the Si (100) substrate are shown in Fig. 1(b) proving that the aligned ZnO NWs are (0002) oriented. The stronger (0002) intensity of ZnO NW arrays indicates that the ZnO NW arrays grew preferentially along the [0001] direction from the seed layer.

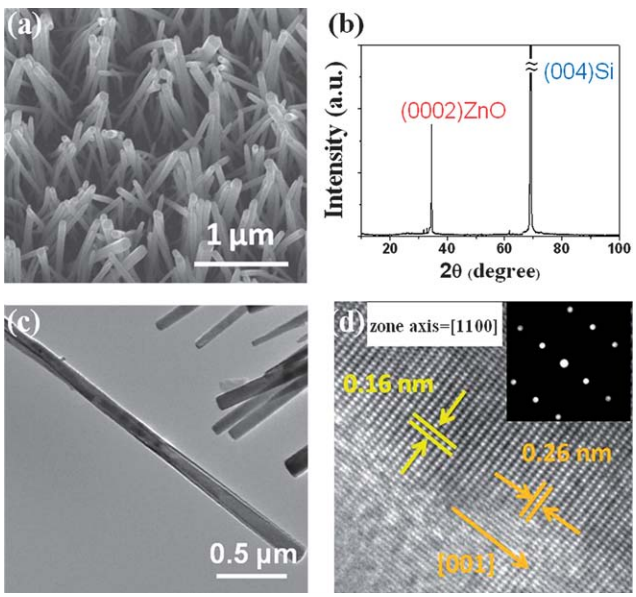

Fig. 1 (a) FESEM image and (b) XRD of the ZnO seed layer and as-grown ZnO NW arrays, respectively. (c) Low-magnification TEM image and (d) HRTEM image of an individual ZnO NW. The inset in (d) is the corresponding FFT diffraction pattern.

The absence of other peaks in the XRD pattern and the narrow full width half maximum value (~0.15°) confirm that these nanostructures were well-aligned.

HRTEM and fast Fourier transformation (FFT) techniques are utilized to obtain more details about the crystal structure of the NWs. Fig. 1(c) shows a TEM image of a single ZnO NW with an aspect ratio of about 28, which is consistent with the FESEM observation. The HRTEM image in Fig. 1(d) depicted a two-dimensional lattice image, confirming the crystallinity. The interplanar spacing was calculated to be 0.26 nm, corresponding to the (0002) plane of the wurtzite structure. By combining the HRTEM images with the FFT diffraction pattern in the inset of Fig. 1(d), we observed the growth of NWs is in the [0001] direction, which is consistent with the result of XRD.

Multistep growth

Compared with vapor phase growth methods of ZnO NWs, the solution growth method contains a finite amount of precursors. Thus, the depletion of the precursors is inevitable, the growth rate decreases as the reaction time increases. The pH value of the solution changes and affects the morphology. Therefore, the aspect ratio of NWs is restricted. In order to improve the aspect ratio of ZnO NWs, multistep growth was adopted to synthesize NWs with higher aspect ratio. The length of ZnO NWs was controlled by the repetitive growth steps with the same growth conditions described above. Fig. 2(a)–(c) show the SEM images of aligned ZnO NW arrays with 1.8 μm, 4.8 μm, and 11.4 μm in length by one step, three steps and five steps, respectively. The diameter also increases with steps of growth, but the lateral growth rate is lower. Therefore, the aspect ratio of the ZnO NWs increases prominently with the increasing steps of growth, resulting in a higher surface-to-volume ratio. The disadvantages of the multistep growth should be pointed out. At each growth step, defects would be introduced at the interfaces/surface between every growth step. With the existence of these defects, the structure of NWs will be deteriorated and defective.

Optical properties

The room temperature PL spectra of aligned ZnO NR arrays grown with different steps are illustrated in Fig. 3. All of the samples show a UV light emission (368–370 nm) and a defect-related emission (420–750 nm). The UV light emission is the intrinsic characteristic of the near-band-edge transition of ZnO.[21] The origin of the defect-related emission is controversial, and several kinds of defects and OH group at the surface are found to be responsible for the emission. In our results, the defect-related emission is enhanced with the steps of growth owing to the increase of the ZnO surface-to-volume ratio and effective area. Additionally, a slight red-shift of defect-related emission is observed. In order to investigate more details of the red-shift

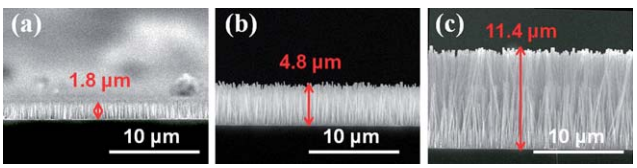

Fig. 2 SEM images of ZnO NW arrays with (a) one step growth, (b) three steps growth, and (c) five steps growth, respectively.

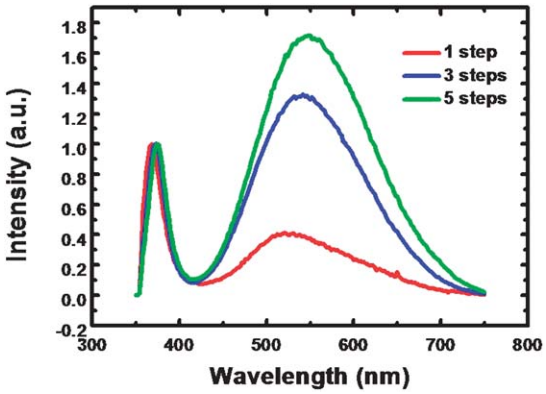

Fig. 3 The room temperature PL spectra of aligned ZnO NW arrays synthesized by one step, three steps, and five steps growth, respectively.

phenomenon, three emission bands (P1 (green emission), P2 (yellow emission), and P3 (red emission)) were adopted to fit the broad visible emission.[22] The results of the three-peak-fitting procedure are illustrated in Fig. 4. With the increase of the multiples of growth, the intensity of all of the peaks increases. However, the increasing amount of the intensity of the peaks is different since the root cause of the emission is different from disparate defects or molecules. The intensity of P2 is increased more than other two peaks and the P2/P1 ratios increase gradually. Since the amount of OH groups is multiplied by the increase of the multiples of growth, the yellow emission band shall be closely related to the OH group. This result and the red-shift effect are identical with the invaluable report by Djurisic *et al.*[23]

Photodetectors

A schematic diagram of a single ZnO NW photodetector device is illustrated in Fig. 5(a) and the inset is the typical SEM image. The scheme demonstrated that Au/Ti electrodes were deposited on the both edges of the ZnO NW. The *I–V* curve shows the functionality of the single ZnO NW device, as illustrated in Fig. 5(b). In this study, the different results of photoresponse can be observed at various biases applied on the photodetector device, 7 V and 5 mV, as shown in Fig. 5(c) and (d), respectively. The response time is defined as the time needed for the photocurrent increasing to 90% of total current variation. Likewise, the reset time is the time needed for the dark current decreasing to 90% of total current variation. The photoresponsivity measurement with a higher bias (7 V) showing the response time and reset time is 5 s and 37 s, as shown in Fig. 5(c), respectively. The reset time of the photocurrents is quite different from high and low bias. The photoconductivity variation is a well-known property of ZnO which implies the electrical conductivity variation owing to the incident radiation.[24] In the dark, oxygen molecules adsorbed on the surface of ZnO NWs and captured free electrons (eqn (1)) that results in a depletion region with low conductivity near the surface.[3] Using the UV illumination, a large number of electron–hole pairs were generated (eqn (2)) which causes the photocurrent to increase. A portion of holes would migrate to the surface of ZnO NWs due to the surface electric field caused by the adsorbed oxygen. The migrated holes neutralized and desorbed the oxygen molecules at the surface (eqn (3)), and the conductivity became higher.

$$O_{2(g)} + e^{-} \rightarrow O_2^{-}{}_{(ad)} \quad (1)$$

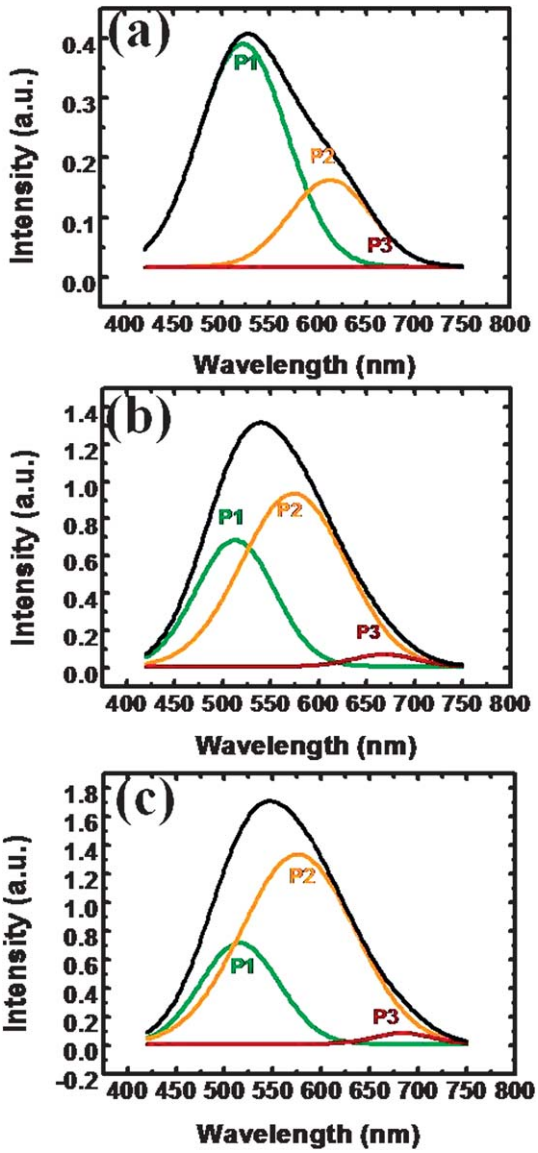

Fig. 4 The defect-related emission analysis of ZnO NWs with (a) one step, (b) three steps, and (c) five steps growth, respectively. The visible emission has been fitted by P1 (~490 to 540 nm), P2 (~555 to 605 nm), and P3 (~655 to 705 nm), respectively.

$$h\nu \rightarrow e^{-} + h^{+} \quad (2)$$

$$h^{+} + O_2^{-}{}_{(ad)} \rightarrow O_{2(g)} \quad (3)$$

The results of the present study provided information regarding the mechanism of reset enhancement with a low bias. Fig. 6 shows the schematic illustration of hole migration when applying different bias under UV illumination. The holes generated by UV illumination were influenced by external electric field and internal electric field, which were individually resulted from bias and surface charge accumulation, respectively. In Fig. 6(a), compared with the internal electric field, the external field with a high bias is so strong that the holes are influenced dramatically. With a high bias, it was hard for the holes to overcome the external electric field and the migration path became

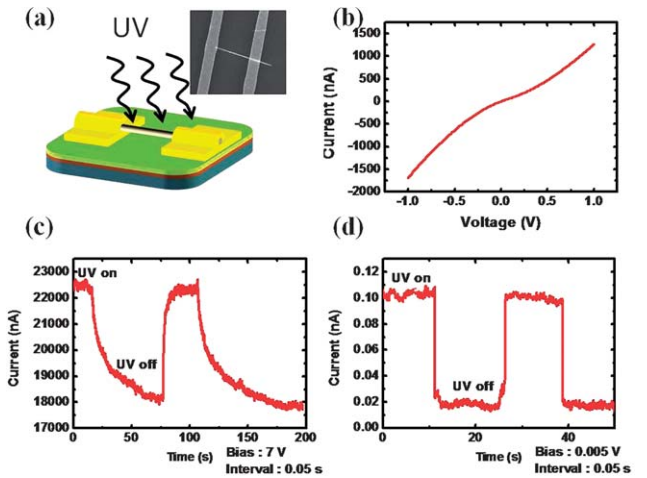

Fig. 5 (a) Schematic illustration and FESEM image of a single ZnO NW photodetector. (b) *I–V* curve of a single ZnO NW measured in the dark. Time-dependent photocurrent response to 365 nm UV with (c) 7 V and (d) 0.005 V bias, respectively.

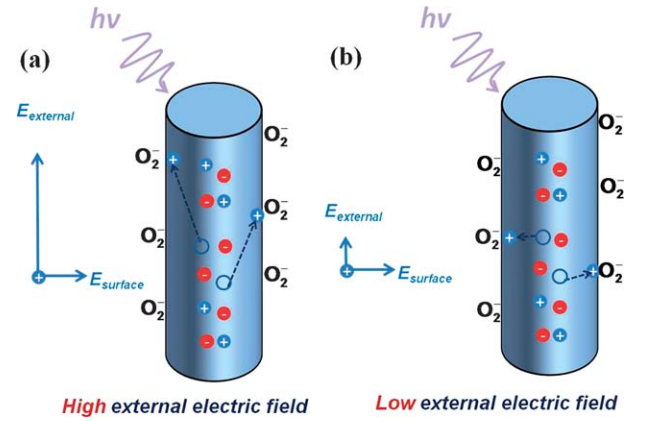

Fig. 6 Schematic illustration of the hole-trapping mechanism of (a) high bias and (b) low bias under UV illumination, respectively.

longer, leading to slower photoresponse. Nevertheless, as shown in Fig. 6(b), a very low bias effectively reduced the energy barrier of hole-trapping. It would be easier for the hole to migrate under a weaker external electric field component, and then the sensitivity of the ZnO NW photodetector could be extremely improved. However, there should be trade-offs between sensitivity and output current. The low external electric field also causes more noisy signals. Furthermore, the influence of bias on the reset time is much dramatic since the reset time is concerning the diffusion of the oxygen molecules to readsorb on the surface of ZnO when the UV is off. At this step, the oxygen molecules capture electrons and the re-adsorb process on the ZnO is more difficult at higher bias due to the higher electron-trapping barrier, resulting in slower response time.

The schematic diagram of an aligned ZnO NWs device and the photoresponsivity measurement are shown in Fig. 7. A 100 nm ZnO seed layer was deposited on the Si substrates and the as-grown ZnO NWs were synthesized with the hydrothermal method. Then, the metal electrodes were fabricated by applying colloidal silver, followed by 150 °C annealing on a hotplate. Similarly, the ultrafast reset time (less than 0.2 s) was obtained with a small bias (1 mV). Unlike the

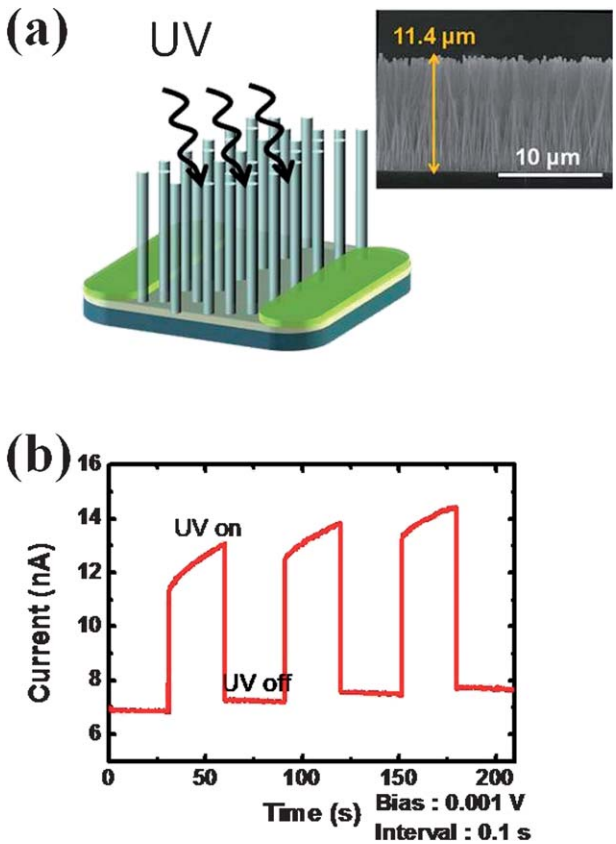

Fig. 7 (a) Schematic illustration and FESEM image of an aligned ZnO NW array photodetector. (b) Time-dependent photocurrent response of a ZnO NW arrays photodetector to 365 nm UV with 1 mV bias.

single ZnO NW photodetector, the current value has a slower saturation after a faster response in the beginning. In comparison with the single NW photodetector, the effective surface area is much larger in the aligned ZnO NWs photodetector. After the rapid photoresponse due to the photogenerated electron–hole pairs, the large amount of adsorbed oxygen makes the photocurrent difficult to saturate and maintains an increase in current.

In particular, the dark current saturation is extremely slow for a NW array photodetector and dark current is inducing a residual current effect when stopping UV illumination.

Conclusions

In summary, ZnO NWs with a [0001] growth direction have been synthesized by the hydrothermal method. The multistep growth was adopted and demonstrated to improve the aspect ratio of ZnO from 22.5 to 57 successfully. From the results of PL spectra, the defect-related emission is enhanced with the increase of the effective surface area, and a red-shift is caused by the occurrence of yellow light emission, which is closely related to the OH group. The photoresponsivity measurements show that the ultrafast reset time was obtained in both single ZnO NW device (<50 ms) and ZnO NW array device (<0.2 s) with a low bias. The highly sensitive photodetector with a low external electric field is attributed to the lower energy barrier of hole-trapping. The result shows an effective method to enhance the sensitivity of the ZnO nanostructure photodetector.

Acknowledgements

The authors would like to acknowledge the support by the National Science Council (grant no. NSC 100-2120-M-007-008, NSC 100-2628-E-009-023-MY3, and NSC 98-2112-M-032-003-MY3).

Notes and references

1 M. H. Huang, S. Mao, H. Feick, H. Q. Yan, Y. Y. Wu, H. Kind, E. Weber, R. Russo and P. D. Yang, *Science*, 2001, **292**, 1897.
2 W. I. Park and G. C. Yi, *Adv. Mater.*, 2004, **16**, 87.
3 W. K. Hong, J. I. Sohn, D. K. Hwang, S. S. Kwon, G. Jo, S. Song, S. M. Kim, H. J. Ko, S. J. Park, M. E. Welland and T. Lee, *Nano Lett.*, 2008, **8**, 950.
4 M. Law, L. E. Greene, J. C. Johnson, R. Saykally and P. D. Yang, *Nat. Mater.*, 2005, **4**, 455.
5 Y. M. Sun, J. W. Seo, C. J. Takacs, J. Seifter and A. J. Heeger, *Adv. Mater.*, 2011, **23**, 1679.
6 J. H. He, Y. H. Lin, M. E. McConney, V. V. Tsukruk, Z. L. Wang and G. Bao, *J. Appl. Phys.*, 2007, **102**, 084303.
7 Q. Wan, Q. H. Li, Y. J. Chen, T. H. Wang, X. L. He, J. P. Li and C. L. Lin, *Appl. Phys. Lett.*, 2004, **84**, 3654.
8 J. H. He, C. H. Ho and C. Y. Chen, *Nanotechnology*, 2009, **20**, 065503.
9 Z. L. Wang and J. H. Song, *Science*, 2006, **312**, 242.
10 L. Vayssieres, *Adv. Mater.*, 2003, **15**, 464.
11 R. B. Peterson, C. L. Fields and B. A. Gregg, *Langmuir*, 2004, **20**, 5114.
12 L. E. Greene, M. Law, J. Goldberger, F. Kim, J. C. Johnson, Y. F. Zhang, R. J. Saykally and P. D. Yang, *Angew. Chem., Int. Ed.*, 2003, **42**, 3031.
13 S. A. Morin, M. J. Bierman, J. Tong and S. Jin, *Science*, 2010, **328**, 476.
14 S. H. Ko, D. Lee, H. W. Kang, K. H. Nam, J. Y. Yeo, S. J. Hong, C. P. Grigoropoulos and H. J. Sung, *Nano Lett.*, 2011, **11**, 666.
15 J. H. Yang, G. M. Liu, J. Lu, Y. F. Qiu and S. H. Yang, *Appl. Phys. Lett.*, 2007, **90**, 103109.
16 M. H. Huang, Y. Y. Wu, H. Feick, N. Tran, E. Weber and P. D. Yang, *Adv. Mater.*, 2001, **13**, 113.
17 B. D. Yao, Y. F. Chan and N. Wang, *Appl. Phys. Lett.*, 2002, **81**, 757.
18 Y. Sun, G. M. Fuge and M. N. R. Ashfold, *Chem. Phys. Lett.*, 2004, **396**, 21.
19 L. Vayssieres, K. Keis, A. Hagfeldt and S. E. Lindquist, *Chem. Mater.*, 2001, **13**, 4395.
20 T. Zhai, L. Li, X. Wang, X. S. Fang, Y. Bando and D. Golberg, *Adv. Funct. Mater.*, 2010, **20**, 4233.
21 Y. Sun, G. M. Fuge, N. A. Fox, D. J. Riley and M. N. R. Ashfold, *Adv. Mater.*, 2005, **17**, 2477.
22 B. Panigrahy, M. Aslam, D. S. Misra, M. Ghosh and D. Bahadur, *Adv. Funct. Mater.*, 2010, **20**, 1161.
23 A. B. Djurisic, Y. H. Leung, K. H. Tam, Y. F. Hsu, L. Ding, W. K. Ge, Y. C. Zhong, K. S. Wong, W. K. Chan, H. L. Tam, K. W. Cheah, W. M. Kwok and D. L. Phillips, *Nanotechnology*, 2007, **18**, 095702.
24 C. Soci, A. Zhang, X. Y. Bao, H. Kim, Y. Lo and D. L. Wang, *J. Nanosci. Nanotechnol.*, 2010, **10**, 1430.

